



## Article

# Influence of Heterointerfaces on the Kinetics of Oxygen Surface Exchange on Epitaxial $\text{La}_{1.85}\text{Sr}_{0.15}\text{CuO}_4$ Thin Films

Gene Yang <sup>1</sup>, So-Yeun Kim <sup>2</sup>, Changhee Sohn <sup>2</sup>, Jong K. Keum <sup>3</sup>  and Dongkyu Lee <sup>1,\*</sup> 

<sup>1</sup> Department of Mechanical Engineering, University of South Carolina, Columbia, SC 29208, USA; geney@email.sc.edu

<sup>2</sup> Department of Physics, Ulsan National Institute of Science and Technology, Ulsan 44919, Korea; soyeun@illinois.edu (S.-Y.K.); chsohn@unist.ac.kr (C.S.)

<sup>3</sup> Center for Nanophase Materials Sciences, Oak Ridge National Laboratory, Neutron Scattering Division, Oak Ridge, TN 37830, USA; keumjk@ornl.gov

\* Correspondence: dongkyu@cec.sc.edu; Tel.: +1-803-777-0084

**Abstract:** Considerable attention has been directed to understanding the influence of heterointerfaces between Ruddlesden–Popper (RP) phases and  $\text{ABO}_3$  perovskites on the kinetics of oxygen electrocatalysis at elevated temperatures. Here, we report the effect of heterointerfaces on the oxygen surface exchange kinetics by employing heteroepitaxial oxide thin films formed by decorating  $\text{LaNiO}_3$  (LNO) on  $\text{La}_{1.85}\text{Sr}_{0.15}\text{CuO}_4$  (LSCO) thin films. Regardless of LNO decoration, tensile in-plane strain on LSCO films does not change. The oxygen surface exchange coefficients ( $k_{\text{chem}}$ ) of LSCO films extracted from electrical conductivity relaxation curves significantly increase with partial decorations of LNO, whereas full LNO coverage leads to the reduction in the  $k_{\text{chem}}$  of LSCO films. The activation energy for oxygen exchange in LSCO films significantly decreases with partial LNO decorations in contrast with the full coverage of LNO. Optical spectroscopy reveals the increased oxygen vacancies in the partially covered LSCO films relative to the undecorated LSCO film. We attribute the enhanced oxygen surface exchange kinetics of LSCO to the increased oxygen vacancies by creating the heterointerface between LSCO and LNO.

**Keywords:** solid oxide fuel cells; cathodes; oxygen reductions reaction; oxygen surface exchange kinetics; electrical conductivity relaxation; oxide thin films;  $\text{ABO}_3$  oxides; Ruddlesden–Popper oxides; surface modification; oxide heterostructures



**Citation:** Yang, G.; Kim, S.-Y.; Sohn, C.; Keum, J.K.; Lee, D. Influence of Heterointerfaces on the Kinetics of Oxygen Surface Exchange on Epitaxial  $\text{La}_{1.85}\text{Sr}_{0.15}\text{CuO}_4$  Thin Films. *Appl. Sci.* **2021**, *11*, 3778. <https://doi.org/10.3390/app11093778>

Academic Editor: Alexander Chroneos

Received: 7 April 2021  
Accepted: 19 April 2021  
Published: 22 April 2021

**Publisher's Note:** MDPI stays neutral with regard to jurisdictional claims in published maps and institutional affiliations.



**Copyright:** © 2021 by the authors. Licensee MDPI, Basel, Switzerland. This article is an open access article distributed under the terms and conditions of the Creative Commons Attribution (CC BY) license (<https://creativecommons.org/licenses/by/4.0/>).

## 1. Introduction

The kinetically sluggish oxygen reduction reaction (ORR) at the cathode primarily limits the efficiency of intermediate temperature solid oxide fuel cells (SOFCs) [1–3], where mixed ionic and electronic conductors (MIECs) such as  $\text{La}_{1-x}\text{Sr}_x\text{Co}_{1-y}\text{FeO}_{3-\delta}$  (LSCF) perovskites are widely used as the cathode [4–6]. Among various approaches to achieve faster ORR activity on the cathode surface, recent studies have focused on forming heterointerfaces between two dissimilar MIECs [7–12]. In particular, oxide heterostructures formed by decorating Ruddlesden–Popper (RP) oxides on  $\text{ABO}_3$  perovskites have enabled the enhancement of the ORR kinetics on  $\text{ABO}_3$  oxides [13–17]. For example, highly enhanced oxygen surface exchange kinetics of  $\text{La}_{0.8}\text{Sr}_{0.2}\text{CoO}_{3-\delta}$  were obtained by synthesizing (001)-oriented multilayer thin films consisting of  $\text{La}_{0.8}\text{Sr}_{0.2}\text{CoO}_{3-\delta}$  and  $\text{LaSrCoO}_{4\pm\delta}$  [17]. Surface decoration on LSCF also effectively increased the ORR kinetics of LSCF [14]. Most of such efforts have been dedicated to improving the ORR kinetics on  $\text{ABO}_3$  by surface modifications with RP oxides. Whereas the mechanism of the enhanced ORR kinetics by the formation of heterointerfaces is not fully understood, the increased interfacial oxygen vacancies are thought to be responsible.

RP oxides are interesting alternative cathode materials to  $\text{ABO}_3$  perovskites due to their controllable stoichiometry (from oxygen excess to oxygen deficiency) and highly

anisotropic oxygen ion migration [6,18–21]. In addition, RP oxides show no discernible cation segregation, which is the major degradation mechanism of  $ABO_3$  oxides [22,23]. Recently,  $La_{2-x}Sr_xCuO_{4\pm\delta}$  has attracted attentions not only because of its comparable oxygen surface exchange kinetics to that of LSCF at intermediate temperatures [24], but also because of its multifunctionality including high  $T_c$  superconductivity [25–27]. In the case of Sr-doped  $La_2CuO_4$ , oxygen vacancies are the majority oxygen defects controlling the ORR kinetics; thus, the larger the oxygen vacancies, the faster the ORR kinetics. In this regard, the heterointerface formed by  $La_{2-x}Sr_xCuO_{4\pm\delta}$  decorated with  $ABO_3$  lead to the enhancement in the ORR kinetics of  $La_{2-x}Sr_xCuO_{4\pm\delta}$ , as oxygen vacancies can increase at the interface between RP phases and  $ABO_3$  [28,29]. Therefore, in order to increase oxygen vacancies at the heterointerface in this system,  $ABO_3$  oxides are required to readily form oxygen vacancies.  $LaNiO_3$  (LNO) can be a suitable candidate within the  $ABO_3$  perovskites since LNO possesses a relatively low formation energy for oxygen vacancies [30]. In particular, the (001) surface of LNO is known to more easily form oxygen vacancies compared with the LNO lattice [31]. Accordingly, LNO has been intensively used in composite oxides for SOFC cathodes. For instance, the cathode performance was significantly enhanced by mixing LNO with  $La_2NiO_{4+\delta}$  (LNO214) as a composite cathode [32]. Furthermore, time-resolved X-ray diffraction showed no substantial barrier to ionic transport at the interface, which might contribute to the enhanced ORR activity of LNO–LNO214 composites [33]. Even though oxygen interstitials are the major defects in LNO214 [34], the contribution of LNO to the enhanced ORR kinetics in LNO–LNO214 composites is not very well understood.

Here, by growing heteroepitaxial oxide thin films formed by  $La_{1.85}Sr_{0.15}CuO_4$  (LSCO) decorated with LNO as a model system, we show that the oxygen surface exchange kinetics of LSCO can be significantly influenced by LNO decorations that enable an increase in the vacancy content in the LSCO films. We demonstrate that partial LNO decorations can increase the oxygen surface exchange coefficients ( $k_{chem}$ ) of the LSCO film, whereas full LNO coverage reduces the  $k_{chem}$  values.

## 2. Materials and Methods

### 2.1. Thin Film Deposition

Epitaxial LSCO thin films of ~60 nm thickness with LNO surface decoration of different thicknesses, from partial to full coverage (~1.5, ~3, and ~15 nm), were grown by pulsed laser deposition (PLD) on single-crystal (001) yttria-stabilized zirconia (YSZ) substrates. A Gd-doped ceria (GDC) buffer layer (~20 nm) was introduced between LSCO and YSZ to prevent the formation of  $La_2Zr_2O_7$  [35]. The YSZ substrate was attached to the PLD substrate holder using a small amount of silver paint for thermal contact. PLD was performed using a KrF excimer laser at  $\lambda = 248$  nm, 10 Hz pulse rate, and 40 mJ pulse energy under an oxygen partial pressure,  $p(O_2)$ , of  $1.3 \times 10^{-4}$  atm (100 mTorr) with GDC at 550 °C, followed by LSCO and LNO at 700 °C. After completing the deposition, the samples were cooled to room temperature in the PLD chamber for 1 h under a  $p(O_2)$  of  $1.3 \times 10^{-4}$  atm (100 mTorr).

### 2.2. Thin Film Characteristics

Oxide phase purity and crystallography of the films were investigated via high-resolution X-ray diffraction (HRXRD) using a four-circle diffractometer. Measurements were performed in the in-plane and out-of-plane configurations. The thickness of the films was characterized by X-ray reflectivity (XRR) measurements.

### 2.3. Oxygen Surface Exchange Kinetics

Electrical conductivity relaxation (ECR) was performed with a source meter (Keithley 2450) via a van der Pauw configuration. Four silver electrodes were painted on the edge of the sample with a separation of 5 mm. The measurements were carried out in the temperature range from 350 to 650 °C. The relaxations were triggered by switching oxygen

partial pressure from 0.5 to 0.01 with different N<sub>2</sub>-O<sub>2</sub> mixtures. The relaxations during oxygen partial pressure changes were fitted to an exponential equation, from which the time constant  $\tau$  was extracted to calculate the oxygen surface exchange coefficient.

#### 2.4. Optical Conductivity

The ellipsometry technique was employed to obtain the optical constants of the films. Two ellipsometric parameters,  $\psi$  ( $\tan\psi$  corresponds to the amplitude ratio between p- and s-polarization light) and  $\Delta$  (phase difference between p- and s- polarization light), for the films and the bare substrate were obtained at room temperature. The incident angle of light was 70 degrees. The ellipsometric parameters of the bare substrate were directly transformed to the real and imaginary parts of optical conductivity. Then, a two-layer model composed of the substrate and the film was constructed to determine the optical conductivity of the films. The thickness of the films was obtained from separate XRR measurements and fixed during fitting. The only variables in this two-layer model were therefore the real and imaginary parts of the optical constants of the film. The Kramers–Kronig condition was forced during the procedure.

### 3. Results

#### 3.1. Thin Film Characteristics

Figure 1a shows the XRD data of the reference LSCO film and LNO-decorated LSCO films. The films clearly show the presence of the  $(00l)_{tetra.}$  peaks of LSCO and  $(00l)_{cubic}$  peaks of GDC and YSZ, indicating that the LSCO films grew epitaxially. With the LNO coverage of 3 nm thickness, the  $(00l)_{pc}$  peaks of LNO become visible. The subscripts *tetra.* and *pc* denote the tetragonal [20,21] and pseudo-cubic [36] notation, respectively. The  $\phi$  scans of the LNO-decorated LSCO films showed that LNO  $(202)_{pc}$ , LSCO  $(103)_{tetra.}$ , GDC  $(202)_{cubic}$ , and YSZ  $(202)_{cubic}$  have strong peaks with four-fold cubic symmetry (Figure 1b), which reveals the in-plane crystallographic relationships between GDC and YSZ (cube-on-cube alignment), LSCO and GDC (in-plane 45° rotation), and LSCO and LNO (no rotation). The measured in-plane lattice parameters of the LSCO films were found to be  $a = 3.801 \text{ \AA}$  for the undecorated LSCO film,  $a = 3.792 \text{ \AA}$  for ~3 nm LNO-decorated LSCO film, and  $a = 3.804 \text{ \AA}$  for ~15 nm LNO-decorated LSCO film, which are slightly larger compared with the literature data ( $a = 3.777 \text{ \AA}$ ,  $c = 13.226 \text{ \AA}$  for bulk LSCO [26]). Considering the lattice mismatch between LSCO and GDC, the LSCO films were tensile-strained, which was further confirmed by XRD reciprocal space maps (RSMs) shown in Figure 1c–e. Therefore, the effect of strain on the oxygen surface exchange kinetics was ruled out in this study.

#### 3.2. Oxygen Surface Exchange Kinetics

Figure 2 shows an ECR normalized curve corresponding to the 0.5 to 0.1 atm of the reduction step measured with the LSCO film decorated with ~3 nm thick LNO at 450 °C. ECR measures the electrical conductivity of the thin film as a function of time during a change in the oxygen partial pressure,  $p(\text{O}_2)$  [37,38]. The electrical conductivity is very sensitive to the changes in oxygen chemical potential depending on the defect chemistry of the thin film, which can enable the evaluation of oxygen transport properties [39,40]. The raw data of the relaxations were fitted by a solution to Fick's second law [41,42]. A simple exponential function

$$g(t) = 1 - \exp\left(-\frac{t}{\tau}\right)$$

with

$$\tau = \frac{l}{k_{\text{chem}}}$$

where  $\tau$ ,  $l$ , and  $k_{\text{chem}}$  are the time constant, film thickness, and oxygen surface exchange coefficient, respectively, was used to fit the experimental results. As shown in Figure 2, the fitted data with the simple model was found to well-match the experimental data, and thus this simple model was used in this work.

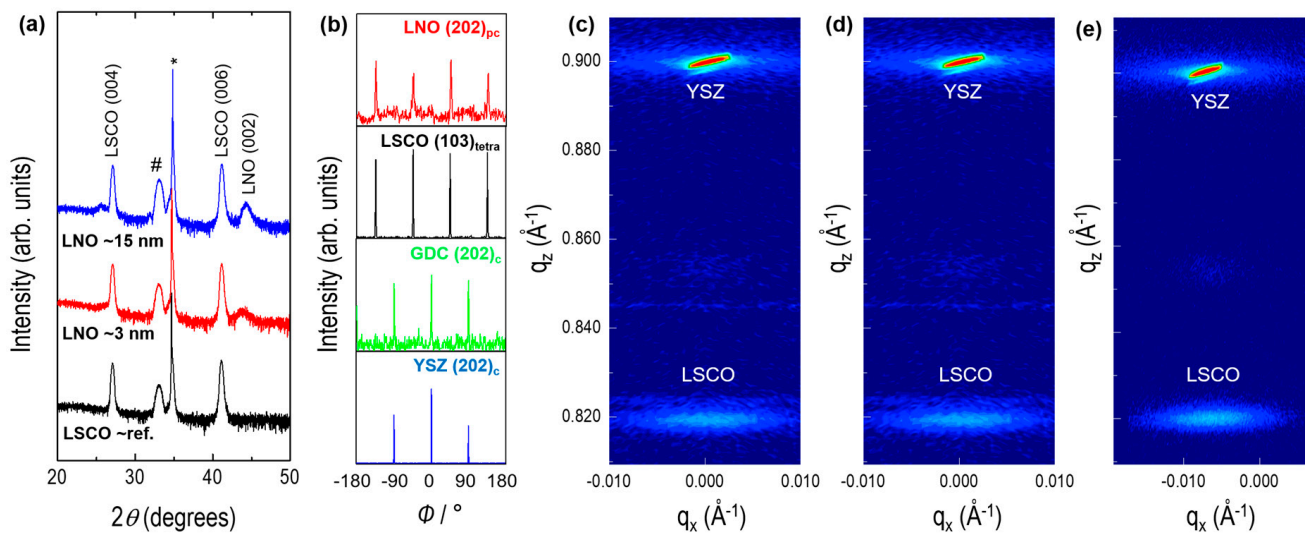


**Figure 1.** (a) XRD  $\theta$ - $2\theta$  patterns of the epitaxial reference LSCO and LNO-decorated LSCO films; (b) XRD  $\phi$  scans of the 202 reflection of a YSZ substrate, a GDC buffer layer ( $\sim 20$  nm), and a LNO film ( $\sim 15$  nm), and of the 103 reflection of a LSCO film ( $\sim 60$  nm). GDC and YSZ substrate peaks are indicated with # and \*, respectively. RSMs around the 2 2-4 Bragg peak from YSZ of (c) reference LSCO, (d)  $\sim 3$  nm LNO-decorated LSCO, and (e)  $\sim 15$  nm LNO-decorated LSCO film.

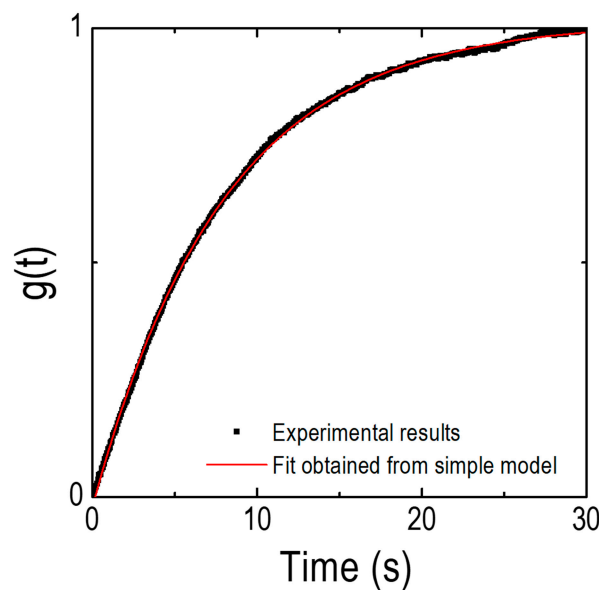


**Figure 2.** Experimental and fitted ECR data obtained from the  $\sim 3$  nm LNO-decorated LSCO film under a gas switch from 0.5 to 0.1 atm at  $450^\circ\text{C}$ .

Figure 3 shows the  $k_{\text{chem}}$  values of the undecorated LSCO and LNO-decorated LSCO films collected from ECR measurements. Considering the film thicknesses were much smaller than the critical thickness (estimated to be  $3\ \mu\text{m}$  for bulk  $\text{La}_2\text{CuO}_4$  [43]), the  $p(\text{O}_2)$ -dependent  $k_{\text{chem}}$  values (Figure 3b) suggest that the oxygen surface exchange kinetics govern the ORR activity on the film surface. As shown in Figure 3, the formation of heterointerfaces has a strong influence on the oxygen surface exchange kinetics of the LSCO film. Interestingly, the  $k_{\text{chem}}$  values of the LSCO films were enhanced with LNO coverage less than or equal to  $\sim 3$  nm in thickness, whereas those were reduced with  $\sim 15$  nm LNO coverage (Figure 3a). Figure 3b shows the  $p(\text{O}_2)$ -dependent  $k_{\text{chem}}$  values of the undecorated LSCO and LNO-decorated LSCO films at  $350^\circ\text{C}$ . At a  $p(\text{O}_2)$  of  $10^{-2}$  atm, the LSCO films with partial LNO coverages showed increased  $k_{\text{chem}}$  values by up to approximately one order of magnitude compared with the undecorated LSCO film. The  $p(\text{O}_2)$  dependency of

$k_{\text{chem}}$  ( $k \propto P_{\text{O}_2}^m$ ) can be indicative of the rate-limiting step of oxygen surface exchange [44,45]. The undecorated LSCO film exhibited an  $m$  value close to 0.5, which indicates that the dissociation of molecular oxygen to atomic oxygen is likely to be the rate-limiting step ( $\text{O}_{2,\text{ads}} \leftrightarrow 2\text{O}_{\text{ads}}$ ). With partial LNO coverages ( $\sim 1.5$  and  $\sim 3$  nm), however, the dependence of  $k_{\text{chem}}$  on  $p(\text{O}_2)$  exhibited noticeable changes. The  $m$  values for the LSCO films with partial LNO coverages were found to be close to 0.25, which implies that the charge transfer process ( $\text{O}_{2,\text{ads}} + 4e^- + 2V_{\text{O}} \leftrightarrow 2\text{O}_{\text{O}^\times}$ ) can be the rate-limiting step. The difference in the rate-limiting step resulting from decorating LNO on LSCO suggests the different amounts of oxygen vacancies in LSCO, since the creation of more oxygen vacancies can provide more active sites for the dissociative adsorption of oxygen. It is therefore hypothesized that the partial LNO surface modifications can increase the concentration of oxygen vacancies on the surface of LSCO film, which may be responsible for the increased oxygen surface exchange rate [46–48]. It is worth noting that the surface oxygen exchange steps proposed in this study may include several elemental steps that might interfere with determining the exact rate-limiting step. However, the different  $m$  values suggest that LNO surface modifications strongly influence the mechanism and kinetics of ORR on the LSCO film. Furthermore, the activation energies for oxygen exchange in the LSCO films with partial LNO decorations were found to be much lower (0.26–0.31 eV) than those in the undecorated LSCO (0.39 eV) and LSCO film with full LNO coverage (0.51 eV). This result clearly shows that the energy barrier for the surface exchange processes of the LSCO film decreased with partial LNO coverages.

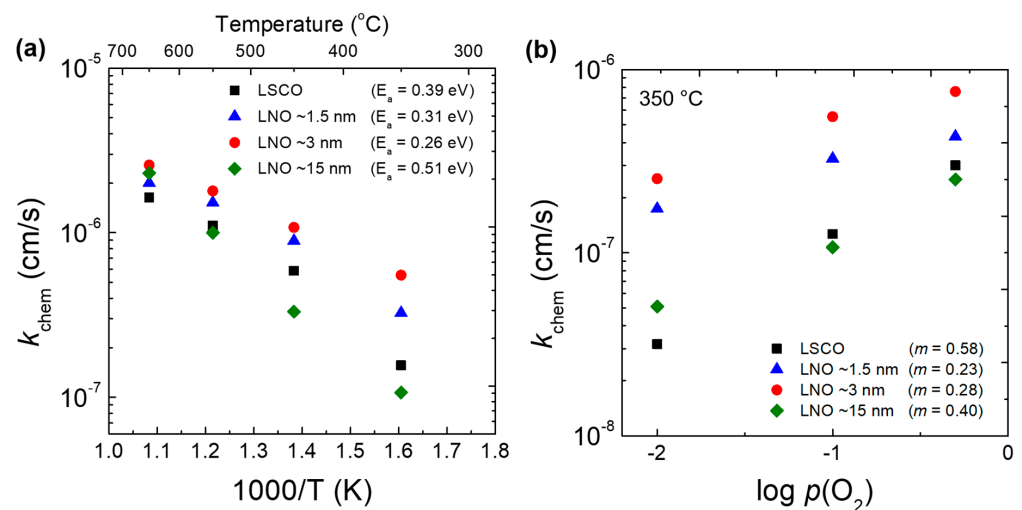


**Figure 3.** (a) Temperature and (b)  $p(\text{O}_2)$ -dependent  $k_{\text{chem}}$  values for undecorated LSCO and LNO-decorated LSCO films.

### 3.3. Optical Conductivity

Since the change in oxygen vacancies can be sensitively examined by optical spectroscopy [49,50], the optical conductivities of the undecorated LSCO and LNO-decorated LSCO films were evaluated by spectroscopic ellipsometry. As shown in Figure 4, a single peak was observed at 1.5 eV for the undecorated LSCO film. The peak position shifted toward lower photon energy with decorating LNO on LSCO. Previous studies also demonstrated a similar trend in the peak shift toward lower photon energy with increasing vacancy contents in  $\text{La}_{2-x}\text{Sr}_x\text{CuO}_4$  [51,52]. Therefore, our optical conductivity results verify the aforementioned hypothesis of the increased oxygen vacancies by forming the heterointerface between LSCO and LNO. The increase in the concentration of oxygen vacancies by decorating LNO on LSCO can also be supported by the theoretical formation energies ( $E_{\text{vac}}$ ) for oxygen vacancies. The formation energy ( $E_{\text{vac}}$ ) for oxygen vacancies in LNO (1.23 eV) is known to be much lower than that in LSCO (2 eV) [24,31]. Accordingly, the LNO-decorated LSCO films have a higher concentration of oxygen vacancies on the surface



compared with the undecorated LSCO film. Given the experimental and theoretical results, the increased oxygen vacancies obtained by constructing the heterointerface between LSCO and LNO facilitate oxygen dissociation and incorporation at the LSCO surface, resulting in the enhancement in ORR activity for the LSCO film.

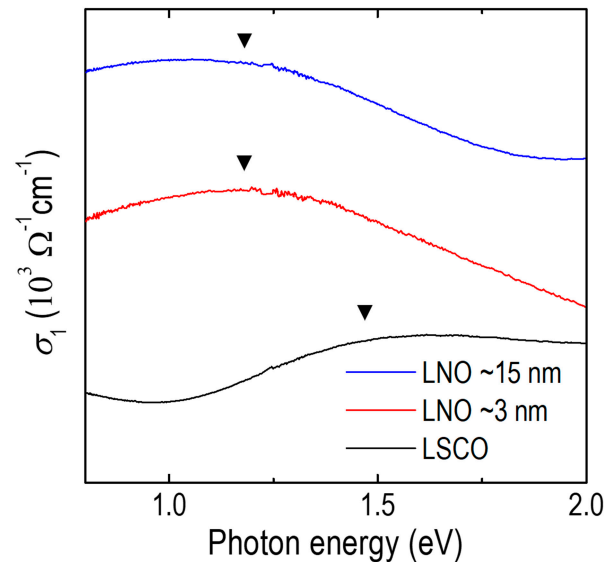


**Figure 4.** Optical conductivity ( $\sigma_1$ ) of the undecorated LSCO and LNO-decorated LSCO films.

#### 4. Discussion

Whereas the LNO surface modification led to an increase in oxygen vacancies in the LSCO films, a fully dense surface layer of LNO was not beneficial for enhancing the oxygen surface exchange kinetics of the LSCO film. As shown in Figure 3, the surface decoration of full LNO coverage was found to be detrimental to the  $k_{chem}$  values of the LSCO film, which cannot be explained by the results from optical spectroscopy. It was reported that the oxygen surface exchange kinetics of oxide thin film heterostructures becomes mainly dependent on decorated materials with increasing thickness of decorated materials [12,13]. Therefore, the decorated LNO becomes more dominant in determining the oxygen surface exchange kinetics of LNO-decorated LSCO films with increasing the LNO thickness. Furthermore, LNO has poor ORR activity at high temperatures due to the decomposition of LNO to  $La_{n+1}Ni_nO_{3n+1}$  and NiO [53] and/or the distorted structure of LNO due to the presence of oxygen vacancies [54,55]. Hence, interfacial LNO/LSCO regions or LNO thin layers of a few nanometers in thickness on LSCO are responsible for the observed ORR kinetics, which is further supported by the  $m$  value of full LNO coverage (~15 nm) being larger than that of the partially covered LSCO films and comparable to a single-layer LNO film ( $m = 0.36$ , not shown in this paper). Consequently, the LSCO films with partial LNO coverages have the charge transfer as the rate-limiting step, whereas the rate-limiting step in the LSCO with full LNO decoration is the same as that in the undecorated LSCO film. Moreover, the activation energy for oxygen exchange in the LSCO with full LNO coverage (0.51 eV) was larger than that in the undecorated LSCO film, which suggests that the thick LNO decoration increased the activation energy barrier for the oxygen exchange of the LSCO film. Therefore, only partial LNO decorations enable the enhancement in the surface exchange kinetics on the LSCO film (Figure 5).

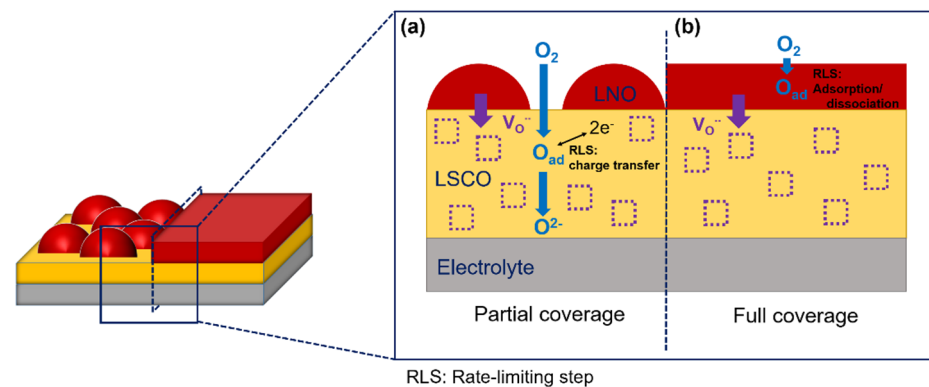


**Figure 5.** Schematic of the surface exchange kinetics of LSCO films with (a) partial LNO coverage and (b) full LNO coverage. The active oxygen vacancies in LSCO with partial LNO coverage lead to fast oxygen incorporation into the LSCO film while full LNO coverage hinders the oxygen incorporation into LSCO.

## 5. Conclusions

In summary, we successfully demonstrated that LNO surface modification can significantly influence the ORR activity of epitaxial LSCO thin films. We showed that the partial LNO decoration (~3 nm) led to enhancement of the  $k_{\text{chem}}$  values of the LSCO films compared with the undecorated LSCO and LSCO with the LNO decoration of full coverage (~15 nm). We also found a change in the rate-limiting step to charge transfer from dissociative adsorption with partial LNO decorations on LSCO. In addition, the activation energies for oxygen exchange in the LSCO films with partial LNO coverages were smaller than those of the undecorated LSCO and LSCO with full LNO coverage. These changes resulted from the increased oxygen vacancies by decorating LNO on LSCO, as confirmed by the optical spectroscopy results. Therefore, the increased oxygen vacancies in the LSCO film promoted the oxygen absorption at the surface, greatly improving the ORR activity. Our results demonstrate the key role of heterointerfaces on the oxygen surface exchange process in RP phases, and a new strategy to design highly active RP oxides for SOFC cathodes.

**Author Contributions:** D.L. and G.Y. designed the idea in this paper. G.Y. performed the experiments and analyzed the data. S.-Y.K. and C.S. performed the optical conductivity experiments. D.L. and G.Y. prepared the first draft. J.K.K. consulted the relevant studies and references. D.L. supervised the paper preparation and finalization. All authors have read and agreed to the published version of the manuscript.

**Funding:** This research was funded by the U.S. Department of Energy (DOE), Office of Science (OS), Basic Energy Sciences (BES), grant number DE-SC0021363. Support for C.S. was provided by Creative Materials Discovery Program through the National Research Foundation of Korea (NRF) funded by Ministry of Science and ICT (NRF-2017M3D1A1040828).

**Institutional Review Board Statement:** Not applicable.

**Informed Consent Statement:** Not applicable.

**Data Availability Statement:** All data are already provided in the manuscript.

**Acknowledgments:** Sample synthesis and structural characterization were performed at the Center for Nanophase Materials Sciences (CNMS), which is sponsored at Oak Ridge National Laboratory (ORNL) by the Scientific User Facilities Division, BES, DOE. Optical spectroscopic studies were conducted at the IBS Center for Correlated Electron Systems, Seoul National University.

**Conflicts of Interest:** The authors declare no conflict of interest.

## References

1. Shao, Z.P.; Haile, S.M. A high-performance cathode for the next generation of solid-oxide fuel cells. *Nature* **2004**, *431*, 170–173. [[CrossRef](#)] [[PubMed](#)]
2. Steele, B.C.H.; Heinzel, A. Materials for fuel-cell technologies. *Nature* **2001**, *414*, 345–352. [[CrossRef](#)] [[PubMed](#)]
3. Shao, M.; Chang, Q.; Dodelet, J.P.; Chenitz, R. Recent advances in electrocatalysts for oxygen reduction reaction. *Chem. Rev.* **2016**, *116*, 3594–3657. [[CrossRef](#)] [[PubMed](#)]
4. Bae, J.M.; Steele, B.C.H. Properties of  $\text{La}_{0.6}\text{Sr}_{0.4}\text{Co}_{0.2}\text{Fe}_{0.8}\text{O}_{3-\delta}$  (LSCF) double layer cathodes on gadolinium-doped cerium oxide (CGO) electrolytes: I. Role of  $\text{SiO}_2$ . *Solid State Ion.* **1998**, *106*, 247–253. [[CrossRef](#)]
5. Esquirol, A.; Brandon, N.P.; Kilner, J.A.; Mogensen, M. Electrochemical characterization of  $\text{La}_{0.6}\text{Sr}_{0.4}\text{Co}_{0.2}\text{Fe}_{0.8}\text{O}_3$  cathodes for intermediate-temperature SOFCs. *J. Electrochem. Soc.* **2004**, *151*, A1847. [[CrossRef](#)]
6. Yang, G.; Jung, W.; Ahn, S.J.; Lee, D. Controlling the oxygen electrocatalysis on perovskite and layered oxide thin films for solid oxide fuel cell cathodes. *Appl. Sci.* **2019**, *9*, 1030. [[CrossRef](#)]
7. Chen, J.; Liang, F.L.; Chi, B.; Pu, J.; Jiang, S.P.; Jian, L. Palladium and ceria infiltrated  $\text{La}_{0.8}\text{Sr}_{0.2}\text{Co}_{0.5}\text{Fe}_{0.5}\text{O}_{3-\delta}$  cathodes of solid oxide fuel cells. *J. Power Sources* **2009**, *194*, 275–280. [[CrossRef](#)]
8. Crumlin, E.J.; Ahn, S.J.; Lee, D.; Mutoro, E.; Biegalski, M.D.; Christen, H.M.; Shao-Horn, Y. Oxygen electrocatalysis on epitaxial  $\text{La}_{0.6}\text{Sr}_{0.4}\text{CoO}_{3-\delta}$  perovskite thin films for solid oxide fuel cells. *J. Electrochem. Soc.* **2012**, *159*, F219–F225. [[CrossRef](#)]
9. Liu, M.F.; Ding, D.; Blinn, K.; Li, X.X.; Nie, L.F.; Liu, M. Enhanced performance of LSCF cathode through surface modification. *Int. J. Hydrogen Energy* **2012**, *37*, 8613–8620. [[CrossRef](#)]
10. Lou, X.; Wang, S.; Liu, Z.; Yang, L.; Liu, M. Improving  $\text{La}_{0.6}\text{Sr}_{0.4}\text{Co}_{0.2}\text{Fe}_{0.8}\text{O}_{3-\delta}$  cathode performance by infiltration of a  $\text{Sm}_{0.5}\text{Sr}_{0.5}\text{CoO}_{3-\delta}$  coating. *Solid State Ion.* **2009**, *180*, 1285–1289. [[CrossRef](#)]
11. Mutoro, E.; Crumlin, E.J.; Biegalski, M.D.; Christen, H.M.; Shao-Horn, Y. Enhanced oxygen reduction activity on surface-decorated perovskite thin films for solid oxide fuel cells. *Energy Environ. Sci.* **2011**, *4*, 3689–3696. [[CrossRef](#)]
12. Lee, D.; Lee, Y.L.; Grimaud, A.; Hong, W.T.; Biegalski, M.D.; Morgan, D.; Shao-Horn, Y. Enhanced oxygen surface exchange kinetics and stability on epitaxial  $\text{La}_{0.8}\text{Sr}_{0.2}\text{CoO}_{3-\delta}$  Thin Films by  $\text{La}_{0.8}\text{Sr}_{0.2}\text{MnO}_{3-\delta}$  Decoration. *J. Phys. Chem. C* **2014**, *118*, 14326–14334. [[CrossRef](#)]
13. Lee, D.; Lee, Y.L.; Hong, W.T.; Biegalski, M.D.; Morgan, D.; Shao-Horn, Y. Oxygen surface exchange kinetics and stability of  $(\text{La,Sr})_2\text{CoO}_{4\pm\delta}/\text{La}_{1-x}\text{Sr}_x\text{MO}_{3-\delta}$  ( $M = \text{Co}$  and  $\text{Fe}$ ) hetero-interfaces at intermediate temperatures. *J. Mater. Chem. A* **2015**, *3*, 2144–2157. [[CrossRef](#)]
14. Lee, D.; Lee, Y.L.; Wang, X.R.; Morgan, D.; Shao-Horn, Y. Enhancement of oxygen surface exchange on epitaxial  $\text{La}_{0.6}\text{Sr}_{0.4}\text{Co}_{0.2}\text{Fe}_{0.8}\text{O}_{3-\delta}$  thin films using advanced heterostructured oxide interface engineering. *MRS Commun.* **2016**, *6*, 204–209. [[CrossRef](#)]
15. Sase, M.; Hermes, F.; Yashiro, K.; Sato, K.; Mizusaki, J.; Kawada, T.; Sakai, N.; Yokokawa, H. Enhancement of oxygen surface exchange at the hetero-interface of  $(\text{La,Sr})\text{CoO}_3/(\text{La,Sr})_2\text{CoO}_4$  with PLD-layered films. *J. Electrochem. Soc.* **2008**, *155*, B793–B797. [[CrossRef](#)]
16. Yashiro, K.; Nakamura, T.; Sase, M.; Hermes, F.; Sato, K.; Kawada, T.; Mizusaki, J. Composite cathode of perovskite-related oxides,  $(\text{La,Sr})\text{CoO}_{3-\delta}/(\text{La,Sr})_2\text{CoO}_{4-\delta}$ , for solid oxide fuel cells. *Electrochem. Solid State Lett.* **2009**, *12*, B135–B137. [[CrossRef](#)]
17. Crumlin, E.J.; Mutoro, E.; Ahn, S.J.; la O', G.J.; Leonard, D.N.; Borisevich, A.; Biegalski, M.D.; Christen, H.M.; Shao-Horn, Y. Oxygen reduction kinetics enhancement on a heterostructured oxide surface for solid oxide fuel cells. *J. Phys. Chem. Lett.* **2010**, *1*, 3149–3155. [[CrossRef](#)]
18. Amow, G.; Skinner, S.J. Recent developments in Ruddlesden-Popper nickelate systems for solid oxide fuel cell cathodes. *J. Solid State Electrochem.* **2006**, *10*, 538–546. [[CrossRef](#)]
19. Burriel, M.; Garcia, G.; Santiso, J.; Kilner, J.A.; Chater, R.J.; Skinner, S.J. Anisotropic oxygen diffusion properties in epitaxial thin films of  $\text{La}_2\text{NiO}_{4+\delta}$ . *J. Mater. Chem. A* **2008**, *18*, 416–422. [[CrossRef](#)]
20. Lee, D.; Lee, Y.L.; Grimaud, A.; Hong, W.T.; Biegalski, M.D.; Morgan, D.; Shao-Horn, Y. Strontium influence on the oxygen electrocatalysis of  $\text{La}_{2-x}\text{Sr}_x\text{NiO}_{4\pm\delta}$  ( $0.0 \leq x_{\text{Sr}} \leq 1.0$ ) thin films. *J. Mater. Chem. A* **2014**, *2*, 6480–6487. [[CrossRef](#)]
21. Lee, D.; Grimaud, A.; Crumlin, E.J.; Mezghani, K.; Habib, M.A.; Feng, Z.; Hong, W.T.; Biegalski, M.D.; Christen, H.M.; Shao-Horn, Y. Strain influence on the oxygen electrocatalysis of the (100)-oriented epitaxial  $\text{La}_2\text{NiO}_{4+\delta}$  thin films at elevated temperatures. *J. Phys. Chem. C* **2013**, *117*, 18789–18795. [[CrossRef](#)]
22. Oh, D.; Gostovic, D.; Wachsman, E.D. Mechanism of  $\text{La}_{0.6}\text{Sr}_{0.4}\text{Co}_{0.2}\text{Fe}_{0.8}\text{O}_3$  cathode degradation. *J. Mater. Res.* **2012**, *27*, 1992–1999. [[CrossRef](#)]
23. Simner, S.P.; Anderson, M.D.; Engelhard, M.H.; Stevenson, J.W. Degradation mechanisms of  $\text{La-Sr-Co-Fe-O}_3$  SOFC Cathodes. *Electrochem. Solid-State Lett.* **2006**, *9*, A478–A481. [[CrossRef](#)]
24. Lee, Y.L.; Lee, D.; Wang, X.R.; Lee, H.N.; Morgan, D.; Shao-Horn, Y. Kinetics of oxygen surface exchange on epitaxial Ruddlesden-Popper phases and correlations to first-principles descriptors. *J. Phys. Chem. Lett.* **2016**, *7*, 244–249. [[CrossRef](#)]
25. Meyer, T.L.; Jacobs, R.; Lee, D.; Jiang, L.; Freeland, J.W.; Sohn, C.; Egami, T.; Morgan, D.; Lee, H.N. Strain control of oxygen kinetics in the Ruddlesden-Popper oxide  $\text{La}_{1.85}\text{Sr}_{0.15}\text{CuO}_4$ . *Nat. Commun.* **2018**, *9*, 92. [[CrossRef](#)]
26. Tarascon, J.M.; Greene, L.H.; Mckinnon, W.R.; Hull, G.W.; Geballe, T.H. Superconductivity at 40 K in the oxygen-defect perovskites  $\text{La}_{2-x}\text{Sr}_x\text{CuO}_{4-y}$ . *Science* **1987**, *235*, 1373–1376. [[CrossRef](#)] [[PubMed](#)]



27. Sato, H. Thickness dependence of superconductivity and resistivity in  $\text{La}_{1.85}\text{Sr}_{0.15}\text{CuO}_4$  films. *Phys. C Supercond.* **2008**, *468*, 991–995. [[CrossRef](#)]
28. Chen, Y.; Chen, Y.; Ding, D.; Ding, Y.; Choi, Y.; Zhang, L.; Yoo, S.; Chen, D.; deGlee, B.; Xu, H.; et al. A robust and active hybrid catalyst for facile oxygen reduction in solid oxide fuel cells. *Energy Environ. Sci.* **2017**, *10*, 964–971. [[CrossRef](#)]
29. Chen, Y.; Yoo, S.; Pei, K.; Chen, D.; Zhang, L.; deGlee, B.; Murphy, R.; Zhao, B.; Zhang, Y.; Chen, Y.; et al. An in situ formed, dual-phase cathode with a highly active catalyst coating for protonic ceramic fuel cells. *Adv. Funct. Mater.* **2018**, *28*, 1704907. [[CrossRef](#)]
30. Lee, Y.L.; Morgan, D.; Kleis, J.; Rossmeis, J. Ab initio defect energetics in  $\text{LaBO}_3$  perovskite solid oxide fuel cell materials. *ECS Trans.* **2019**, *25*, 2761–2767. [[CrossRef](#)]
31. Pan, C.C.; Chen, Y.H.; Wu, N.; Zhang, M.L.; Yuan, L.H.; Zhang, C.R. First-principle study of O vacancy on  $\text{LaNiO}_3$  (001) surface. *Int. J. Hydrogen Energy* **2016**, *41*, 15756–15763. [[CrossRef](#)]
32. Lu, L.; Guo, Y.; Zhang, H.; Jin, J. Electrochemical performance of  $\text{La}_2\text{NiO}_{4+\delta}\text{-La}_{0.6}\text{Sr}_{0.4}\text{Co}_{0.2}\text{Fe}_{0.8}\text{O}_{3-\delta}$  composite cathodes for intermediate temperature solid oxide fuel cells. *Mater. Res. Bull.* **2010**, *45*, 1135–1140. [[CrossRef](#)]
33. Moreno, R.; García, P.; Zapata, J.; Roqueta, J.; Chaigneau, J.; Santiso, J. Chemical strain kinetics induced by oxygen surface exchange in epitaxial films explored by time-resolved X-ray diffraction. *Chem. Mater.* **2013**, *25*, 3640–3647. [[CrossRef](#)]
34. Lee, D.; Lee, H.N. Controlling oxygen mobility in Ruddlesden-Popper oxides. *Materials* **2017**, *10*, 368. [[CrossRef](#)]
35. Mitterdorfer, A.; Gauckler, L.J.  $\text{La}_2\text{Zr}_2\text{O}_7$  formation and oxygen reduction kinetics of the  $\text{La}_{0.85}\text{Sr}_{0.15}\text{Mn}_y\text{O}_3$ ,  $\text{O}_2(\text{g})$  | YSZ system. *Solid State Ion.* **1998**, *111*, 185–218. [[CrossRef](#)]
36. la O', G.J.; Ahn, S.J.; Crumlin, E.; Orikasa, Y.; Biegalski, M.D.; Christen, H.M.; Shao-Horn, Y. Catalytic activity enhancement for oxygen reduction on epitaxial perovskite thin films for solid-oxide fuel cells. *Angew. Chem. Int. Ed.* **2010**, *49*, 5344–5347. [[CrossRef](#)]
37. Ma, B.; Balachandran, U.; Park, J.H.; Segre, C.U. Determination of chemical diffusion coefficient of  $\text{SrFeCo}_{0.5}\text{O}_x$  by the conductivity relaxation method. *Solid State Ion.* **1996**, *83*, 65–71. [[CrossRef](#)]
38. Murugaraj, R.; Govindaraj, G.; Suganthi, R.; George, D. Electrical conductivity studies of sodium borate system based on diffusion controlled relaxation model. *J. Mater. Sci.* **2003**, *38*, 107–112. [[CrossRef](#)]
39. Chen, X.J.; Soltan, S.; Zhang, H.; Habermeier, H.U. Strain effect on electronic transport and ferromagnetic transition temperature in  $\text{La}_{0.9}\text{Sr}_{0.1}\text{MnO}_3$  thin films. *Phys. Rev. B* **2002**, *65*, 174402. [[CrossRef](#)]
40. Mosleh, M.; Søgaard, M.; Hendriksen, P.V. Kinetics and mechanisms of oxygen surface exchange on  $\text{La}_{0.6}\text{Sr}_{0.4}\text{FeO}_{3-\delta}$  thin films. *J. Electrochem. Soc.* **2009**, *156*, B441–B457. [[CrossRef](#)]
41. Crank, J. *The Mathematics of Diffusion*; Clarendon Press: Oxford, UK, 1975.
42. Garcia, G.; Burriel, M.; Bonanos, N.; Santiso, J. Electrical conductivity and oxygen exchange kinetics of  $\text{La}_2\text{NiO}_{4+\delta}$  thin films grown by chemical vapor deposition. *J. Electrochem. Soc.* **2008**, *155*, P28–P32. [[CrossRef](#)]
43. Boehm, E.; Bassat, J.M.; Steil, M.C.; Dordor, P.; Mauvy, F.; Grenier, J.C. Oxygen transport properties of  $\text{La}_2\text{Ni}_{1-x}\text{Cu}_x\text{O}_{4+\delta}$  mixed conducting oxides. *Solid State Sci.* **2003**, *5*, 973–981. [[CrossRef](#)]
44. De Souza, R.A. A universal empirical expression for the isotope surface exchange coefficients ( $k^*$ ) of acceptor-doped perovskite and fluorite oxides. *Phys. Chem. Chem. Phys.* **2006**, *8*, 890–897. [[CrossRef](#)] [[PubMed](#)]
45. Adler, S.B.; Chen, X.Y.; Wilson, J.R. Mechanisms and rate laws for oxygen exchange on mixed-conducting oxide surfaces. *J. Catal.* **2007**, *245*, 91–109. [[CrossRef](#)]
46. Adler, S.B. Factors governing oxygen reduction in solid oxide fuel cell cathodes. *Chem. Rev.* **2004**, *104*, 4791–4844. [[CrossRef](#)] [[PubMed](#)]
47. Choi, Y.; Lynch, M.E.; Lin, M.C.; Liu, M. Prediction of  $\text{O}_2$  dissociation kinetics on  $\text{LaMnO}_3$ -based cathode materials for solid oxide fuel cells. *J. Phys. Chem. C* **2009**, *113*, 7290–7297. [[CrossRef](#)]
48. Zhao, C.; Liu, X.; Zhang, W.; Zheng, Y.; Li, Y.; Yu, B.; Wang, J.; Chen, J. Measurement of oxygen reduction/evolution kinetics enhanced  $(\text{La,Sr})\text{CoO}_3/(\text{La,Sr})_2\text{CoO}_4$  hetero-structure oxygen electrode in operating temperature for SOCs. *Int. J. Hydrogen Energy* **2018**, *44*, 19102–19112. [[CrossRef](#)]
49. Choi, W.S.; Kwon, J.H.; Jeon, H.; Hamann-Borrero, J.E.; Radi, A.; Macke, S.; Sutarto, R.; He, F.; Sawatzky, G.A.; Hinkov, V.; et al. Strain-induced spin states in atomically ordered cobaltites. *Nano Lett.* **2012**, *12*, 4966–4970. [[CrossRef](#)] [[PubMed](#)]
50. Lee, D.; Jacobs, R.; Jee, Y.; Seo, A.; Sohn, C.; Ievlev, A.V.; Ovchinnikova, O.S.; Huang, K.; Morgan, D.; Lee, H.N. Stretching epitaxial  $\text{La}_{0.6}\text{Sr}_{0.4}\text{CoO}_{3-\delta}$  for fast oxygen reduction. *J. Phys. Chem. C* **2017**, *121*, 25651–25658. [[CrossRef](#)]
51. Uchida, S.; Ido, T.; Takagi, H.; Arima, T.; Tokura, Y.; Tajima, S. Optical spectra of  $\text{La}_{2-x}\text{Sr}_x\text{CuO}_4$ : Effect of carrier doping on the electronic structure of the  $\text{CuO}_2$  plane. *Phys. Rev. B* **1991**, *43*, 7942–7954. [[CrossRef](#)]
52. Comanac, A.; de' Medici, L.; Capone, M.; Millis, A.J. Optical conductivity and the correlation strength of high-temperature copper-oxide superconductors. *Nat. Phys.* **2008**, *4*, 287–290. [[CrossRef](#)]
53. Höfer, H.E.; Kock, W.F. Crystal chemistry and thermal behavior in the  $\text{La}(\text{Cr}, \text{Ni})\text{O}_3$  perovskite system. *J. Electrochem. Soc.* **1993**, *140*, 2889–2894. [[CrossRef](#)]
54. Fierro, J.L.G.; Tascón, J.M.D.; Tejuca, L.G. Surface properties of  $\text{LaNiO}_3$ : Kinetic studies of reduction and of oxygen adsorption. *J. Catal.* **1985**, *93*, 83–91. [[CrossRef](#)]
55. Retuerto, M.; Pereira, A.G.; Pérez-Alonso, F.J.; Peña, M.A.; Fierro, J.L.G.; Alonso, J.A.; Fernández-Díaz, M.T.; Pascual, L.; Rojas, S. Structural effects of  $\text{LaNiO}_3$  as electrocatalyst for the oxygen reduction reaction. *Appl. Catal. B* **2017**, *203*, 363–371. [[CrossRef](#)]